2015

Drag from fishing gear entangling North Atlantic right whales

Julie M. van der Hoop
Massachusetts Institute of Technology-Woods Hole Oceanographic Institution Joint Program in Oceanography/Applied Ocean Science and Engineering, Cambridge, Massachusetts

Peter Corkeron
NOAA Fisheries, Northeast Fisheries Science Center, Woods Hole, Massachusetts

John Kenney
NOAA Fisheries, Greater Atlantic Regional Office, Saunderstown, Rhode Island

Scott Landry
Center for Coastal Studies, Provincetown, Massachusetts

David Morin
NOAA Fisheries, Greater Atlantic Regional Office, Gloucester, Massachusetts

See next page for additional authors

Authors
Julie M. van der Hoop, Peter Corkeron, John Kenney, Scott Landry, David Morin, Jamison Smith, and Michael J. Moore

Marine Mammal Science

MARINE MAMMAL SCIENCE, **(*): ***–*** (*** 2015)

DOI: 10.1111/mms.12292

published online : 9 DEC 2015

Drag from fishing gear entangling North Atlantic right whales

Julie M. van der Hoop,[1] Massachusetts Institute of Technology-Woods Hole Oceanographic Institution Joint Program in Oceanography/Applied Ocean Science and Engineering, 77 Massachusetts Avenue, Cambridge, Massachusetts, 02139, U.S.A. and Woods Hole Oceanographic Institution, 266 Woods Hole Road MS 50, Woods Hole, Massachusetts 02543, U.S.A.; **Peter Corkeron,** NOAA Fisheries, Northeast Fisheries Science Center, Woods Hole, Massachusetts 02543, U.S.A.; **John Kenney,** NOAA Fisheries, Greater Atlantic Regional Office, Saunderstown, Rhode Island 02874, U.S.A.; **Scott Landry,** Center for Coastal Studies, 5 Holway Avenue, Provincetown, Massachusetts 02657, U.S.A.; **David Morin and Jamison Smith,** NOAA Fisheries, Greater Atlantic Regional Office, 55 Great Republic Drive, Gloucester, Massachusetts 01930, U.S.A.; **Michael J. Moore,** Woods Hole Oceanographic Institution, 266 Woods Hole Road MS 50, Woods Hole, Massachusetts 02543, U.S.A.

Abstract

Lethal and sublethal fishing gear entanglement is pervasive in North Atlantic right whales (*Eubalaena glacialis*). Entanglement can lead to direct injury and is likely to incur substantial energetic costs. This study (1) evaluates drag characteristics of entangled right whales, (2) contextualizes gear drag measurements for individual whales, and (3) quantifies the benefits of partial disentanglement. A load cell measured drag forces on 15 sets of fishing gear removed from entangled right whales, a towed satellite telemetry buoy, and 200 m of polypropylene line as it was shortened to 25 m, as they were towed behind a vessel at ~0.77, 1.3, and 2.1 m/s (~1.5, 2.5, and 4 knots) and ~0, 3, and 6 m depth. Mean drag ranges from 8.5 N to 315 N, and can be predicted from the dry weight or length of the gear. Combining gear drag measurements with theoretical estimates of drag on whales' bodies suggests that on average, entanglement increases drag and propulsive power by 1.47 fold. Reducing trailing line length by 75% can reduce parasitic gear drag by 85%, reinforcing current disentanglement response practices. These drag measurements can be incorporated into disentanglement response, serious injury determination, and evaluation of sublethal effects on population dynamics.

Key words: whale, fisheries, rope, thrust, line, drag coefficient, energetics.

Lethal and sublethal trauma to North Atlantic right whales (hereafter right whales; *Eubalaena glacialis*) from entanglement in fishing gear is pervasive in this endangered species (Knowlton *et al.* 2012, van der Hoop *et al.* 2013*a*). The majority of recorded right whale entanglement cases involve free-swimming whales that are no longer anchored by gear (NMFS 2003). The impacts of

[1]Corresponding author (e-mail: jvanderhoop@whoi.edu).

entanglement can then become protracted as portions of the entangling gear are carried for months to years (Moore *et al.* 2006, Moore and van der Hoop 2012). Entangling gear may wrap and abrade body parts, while towing large portions of trailing gear likely affects an individual's energy balance: emaciation was documented in 56% of a case series of entanglement mortalities (Cassoff *et al.* 2011).

That emaciation is so commonly reported in chronic entanglement cases is not surprising. The theoretical basis is that towed bodies add drag to the system (Fridman and Dvernik 1973, Batchelor 2000), which then requires more thrust for forward movement, involving additional energy output by the animal (Webb 1975). The literature on scientific instrumentation ethics provides direct evidence for changes in body condition associated with drag and weight of tags (*e.g.*, reviewed in Barron *et al.* 2010). While the energetic consequences imposed by entangling fishing gear have been described (Fowler 1987, Wells *et al.* 2008, Barco *et al.* 2010, Cassoff *et al.* 2011, Wegner and Cartamil 2012, Barratclough *et al.* 2014), only recently have they been quantified (Feldkamp *et al.* 1988, van der Hoop *et al.* 2013*b*). van der Hoop *et al.* (2013*b*) showed that towing gear increased power requirements of one entangled right whale by 70% to 102% when maintaining preferred swimming speeds. Quantifying the parasitic drag imposed by entangling gear is the first step in evaluating these energetic impacts, and is critical in assessing the potential for survival and recovery of an entangled whale.

Disentanglement groups (*e.g.,* the Center for Coastal Studies, CCS; Provincetown, MA) and networks (*e.g.,* the Atlantic Large Whale Disentanglement Network, ALWDN [USA]; International Whaling Commission Global Whale Entanglement Response Network) have been established to train responders to address the growing number of whale entanglements reported worldwide. Ultimately, disentanglement response seeks to reduce the potentially lethal portions of gear (not necessarily all gear) while maintaining high human and whale safety (IWC 2011). While new tools for at-sea tranquilization (Moore *et al.* 2010) and gear removal (Moore *et al.* 2012) have been developed to enhance disentanglement effectiveness, success continues to vary, often requiring multiple disentanglement attempts, especially in right whales. Satellite telemetry buoys (Fig. S1) are sometimes attached to trailing gear to track whales until conditions (*e.g.*, equipment, personnel, weather or time of day) favor further attempts at gear removal. In some attempts, trailing gear is cut to minimize the risk of further entanglement and to reduce parasitic drag and energetic impacts, especially in chronic entanglement cases.

The fishing gear removed through disentanglement operations can and should be archived and studied to better understand the causes and effects of entanglement (Johnson *et al.* 2005, Knowlton *et al.* 2015). To quantify the amount of drag imposed by entangling gear, and the energetic impacts potentially incurred, a load cell tensiometer measured drag forces (Fig. 1) from 15 sets of fishing gear removed from entangled whales (Fig. 2, S2), and an additional six sets similar to those found on entangling whales (21 total configurations). This study (1) describes and compares the drag characteristics of sets of fishing gear entangling right whales, (2) puts the drag measurements in the context of individual whales entangled by the gear, and (3) quantifies the benefits of partial gear removal.

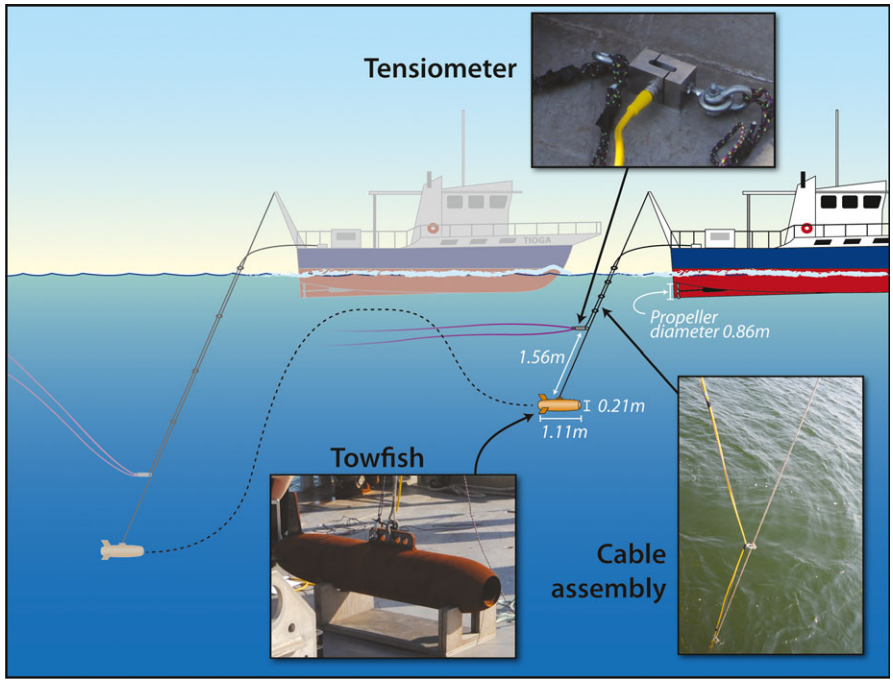

Figure 1. The experimental setup. The towfish is towed from the R/V *Tioga*, below the tensiometer's attachment to fishing gear (orange and purple lines). The winch line controls the depth of the towfish, from 0 to 6 m measured at the depth of the tensiometer. Changing the depth of the towfish has an effect on the gear's orientation in the water column (orange *vs.* purple gear).

Methods

Experimental Gear Description

Fifteen sets of fishing gear removed from past entanglements of right whales were selected from those available through the NOAA (National Oceanic and Atmospheric Administration) Gear Research Team; and where whale ID, specific entanglement dates, and individual fate were known. Chain-of-custody protocols were followed during all transfers. Some gear sets had been altered to return components to their rightful owner, or for use in other previous experiments. Gear sets were reassembled as needed, and towed in configurations that best replicated the entanglement scenario of each case as documented by the disentanglement team (see, *e.g.*, Fig. 2) as practical.

Two additional set-ups were measured: (1) 200 m of 8 mm diameter polypropylene line as it was successively shortened to 25 m, and (2) a satellite telemetry buoy (Fig. S1) used in relocating entangled whales by members of the ALWDN (http://www.nero.noaa.gov/whaletrp/plan/disent/). The satellite telemetry buoy is a 0.36 m diameter deep-water trawl buoy rated to 600 m, fitted with a stainless steel counterbalanced harness for satellite and VHF radio telemetry transmitters. The buoy is appropriately weighted and designed to retain an upward orientation, to allow for satellite and radio communication, when towed at speeds of up to 3.6 m/s, or when

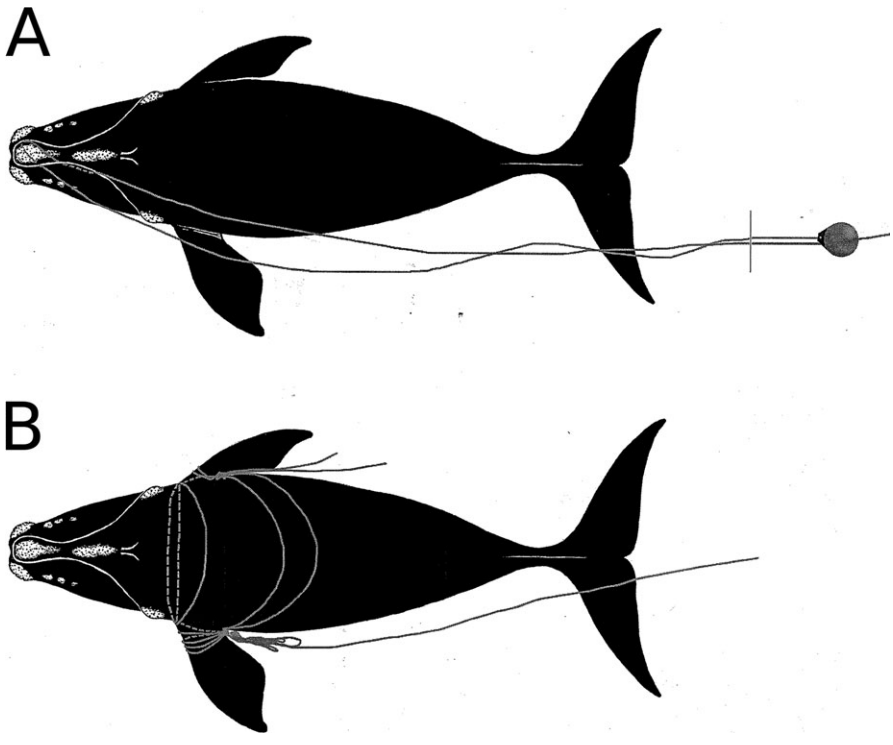

Figure 2. Entangling gear can have very different configurations on North Atlantic right whales. A. EG 1427, showing a rostrum wrap with 82 m (269 ft) of trailing line. B. EG 2030, showing extensive body and flipper wraps, with little line trailing. Dashed lines are used to illustrate rope on the underside of the animal.

floating carrying up to 6.8 kg of entangling gear and attachment hardware, should it come free from a whale.

Tow Experiment

On 12 September 2012, the 15 sets of fishing gear removed from right whales, 8 mm diameter line, and a satellite telemetry buoy (Fig. S1) were towed behind the R/V *Tioga* in Buzzards Bay, Massachusetts, to measure drag forces with a tensiometer (Fig. 1; van der Hoop *et al.* 2013*b*). The R/V *Tioga* is an 18.3 m (60 ft) motorized vessel (5.2 m [17 ft] beam and 1.5 m [5 ft] draft) with Twin Series 60 Detroit Diesel 750 horsepower engines. At the transom, the *Tioga's* stern hull is 0.84 m below the mean waterline, and the hubs of the 0.86 m diameter propellers sit 0.68 m below the mean waterline (Fig. 1). Average wind speeds were 6 km/h. Slack water occurred at 8:14, and maximum current speeds of 1.0 knot (0.5 m/s) were reached at 1040 before the next slack water at 1421. All gear sets were towed between the hours of 0914 and 1500.

Each set of fishing gear was attached to an HRS-1K load cell tensiometer (Load Cell Central, Monroeton, PA; Fig. 1), connected to a towline 1.56 m above a 1.1 m long × 0.21 m diameter tow fish (Fig. 1). The load cell was therefore located outside of (above) the hydrodynamic influence of the tow fish, but within the draft of the

vessel. The cable to the load cell was tied to a 4 mm line attached to 12 shackles closed around the winch cable (Fig. 1). This thin line could then be hauled in, similar to a shower curtain, to allow the load cell to be retrieved without cable strain. The load cell was connected to a laptop computer through a WeightSense OM-232-D Digital Signal Conditioner and read through custom graphical user interface software (ScaleWatch LITE, Load Cell Central, Monroeton, PA), sampling at 60 Hz, and accurate to ±0.14 kg.

Drag on each gear set was measured at three speeds: approximately 1.5, 2.5, and 4.0 knots (0.77, 1.3, and 2.1 m/s). Speed over ground was measured by a shipboard GPS (NavNet VX2; Furuno USA, Camas, WA) at 1 Hz, and handheld GPS (Triton 1500; Magellan Navigation, San Dimas, CA) at approximately 3.05 Hz (range 0.5–60 Hz). Speed through the water was calculated by subtracting current speeds measured by a shipboard ADCP (300 KHz WorkHorse Mariner, Teledyne RDI Instruments, Poway, CA). At each speed, gear sets were towed at depths of 0 m, 3 m, and 6 m, measured at 1 Hz by a ReefNet Sensus Pro depth recorder (Mississauga, ON, Canada). Depth was limited by the cable length and pressure sensitivity of the load cell. It was expected that drag would increase with depth, as an increasing angle between rope and flow direction would lead to a greater projected frontal area as gear is buoyed to the surface (*e.g.*, Fig 1).

Analysis

Mean (± SD) drag forces were calculated from the tensiometer measurements over the 30 s period with the lowest variance in drag for each depth and speed combination ($n = 9$ measurement points per gear set). Doing so isolated the measurement period to one where drag measurements were most stable, to reduce variability introduced by current flow and/or turbulence, and where vessel speed and tow depth were not intentionally being changed. The relationship between drag and speed at each depth was fit with a power model for each tow based on theory.

Gear sets removed from whales ($n = 15$) were weighed and measured when dry, prior to towing. The relationship between average drag measured across all depths and speeds and the dry weight (kg) was fit with a linear model; the presence of floats or buoys was added as a complex covariate for the relationship between drag and length (m) of a gear set ($n = 21$). ANOVA was used to test for a difference in slopes between gear sets with and without floats. Outliers were detected and removed when Cook's $D > 4/n$ (Mendenhall and Sincich 2011).

Entangling Gear Description

A list of symbols, abbreviations, and units are provided in Table 1. From measured drag values, the drag coefficient (C_d; dimensionless) of each gear set at each measurement point was estimated by

$$C_d = \frac{2DG}{\rho U^2 A}, \tag{1}$$

where DG is the drag force (N) on the gear measured from the tensiometer, ρ is seawater density (1,025 kg/m^3), U is the tow speed (m/s), and A is the wetted surface area (m^2) of the gear set. Wetted surface area was estimated based on the area of a cylinder with a specified length, l, and radius, r:

Table 1. List of symbols and abbreviations.

Symbol	Definition (unit)
A	Wetted surface area (m^2)
C_d	Drag coefficient
C_{dI}	Interference drag coefficient
C_f	Friction coefficient
d	Body diameter (m)
d_{max}	Maximum body diameter (m)
DG	Tensiometer-measured gear drag (N)
DI	Interference drag (N)
DW	Total whale drag (N)
F	Theoretical drag force (N)
g	Appendage drag augmentation factor
h	Height of gear off body (m)
l	Length (m)
P_p	Propulsive power (W)
r	Radius (m)
Re	Reynolds number
U	Speed (m/s)
v	Kinematic viscosity (m^2/s)
W	Weight (kg)
δ	Boundary layer thickness (m)
γ	Surface wave drag factor
η	Efficiency coefficient
ρ	Seawater density (kg/m^3)

$$A = 2\pi rl. \tag{2}$$

For most gear sets, this calculation was straightforward and based on the single line diameter and dimensions; however, six gear sets consisted of multiple line types, floats, or buoys, and total wetted surface area was estimated as the sum of surface areas of the components of each gear set. For all attached floats and buoys, half of the wetted surface area was calculated, assuming that half of each item was submerged (see Appendix S1).

The Reynolds number of each gear set was calculated as

$$Re = \frac{lU}{v}, \tag{3}$$

where v is the kinematic viscosity for 16°C seawater (1.17×10^{-6} m^2/s).

To compare the relative influence of surface wave drag, the Froude number (Fn; dimensionless) was calculated for floats on certain gear sets, including the telemetry buoy (see Appendix S1), across the range of measured tow speeds (U; m/s) as

$$Fn = \frac{U}{\sqrt{gl}},$$

where g is the acceleration due to gravity (9.8 m/s^2) and l is the length of the float (m) at the water line level, assuming that each float is half submerged.

To determine whether certain gear configurations have similar drag coefficients or responses to depth and speed, hierarchically clustering using Manhattan distance dissimilarity metric and Ward's minimal variance clustering algorithm were performed in R (Warnes *et al.* 2014). Within identified clusters, the effects of depth and speed are described, including their relative influences, calculated as the percent change in drag coefficient for each gear set between different levels of depth and speed.

Effect of Partial Gear Removal

To determine the incremental effect of line length on drag, a piece of 8 mm diameter polypropylene line was repeatedly measured on the tow cell as it was shortened in stages from 200 m to 25 m in length (200, 150, 100, 50, 25 m). Power functions were fit to mean drag measurements across measured speeds for each length of line. Due to significant effects of depth (see Results), only surface drag measurements were used. From these curves, the percent reduction in drag was calculated between decreasing lengths of line, across speeds of 0.2 to 2.15 m/s.

Entangled Whale Drag

The drag on each whale entangled by the 15 sets of fishing gear towed was estimated to illustrate the relative contribution of drag from gear to the entangled whale system (Rayleigh 1876, Batchelor 2000).

The theoretical rigid-body drag force (F; N) was calculated based on a turbulent spindle model (Webb 1975),

$$F = \frac{1}{2}\rho U^2 A C_d, \tag{4}$$

where ρ is seawater density (1,025 kg/m^3), U is swimming speed (m/s), and A is the total wetted surface area (m^2) calculated from body weight W (kg) as $A = 0.08W^{0.65}$ (Fish 1993). C_d is the drag coefficient, calculated as

$$C_d = C_f\left[1 + 1.5\left(\frac{d_{\max}}{l}\right)^{3/2} + 7\left(\frac{d_{\max}}{l}\right)^{3}\right], \tag{5}$$

where C_f is the frictional drag component computed from the Reynolds number (Re),

$$C_f = 0.072(Re^{-\frac{1}{5}}), \tag{6}$$

and $d_{\max}$ and l are the maximum body diameter (m) and total body length (m).

Body dimensions were obtained for each individual whale (Table 2). Body length (cm) and weight (kg) were estimated from age at the first sighting of entanglement based on Moore *et al.* (2004). For four individuals, birth year was not known. Length and weight were estimated from minimum age in two cases (Egs 1102 and 3294), and expected ages based on size-at-age approximations by staff at the New England Aquarium in the two other cases. The minimum age of Eg 3610, estimated to be a juvenile, was increased from 1 to 3 yr. Eg 2030 was identified as an adult; her estimated age was therefore increased from 9 to 12 yr, the age at which right whales attain 95% of their total body length (Fortune *et al.* 2012). Maximum body diameter

Table 2. Catalog identification number, entangling gear identification number, age, and estimated length (m) and weight (kg; from Moore *et al.* 2004) of North Atlantic right whales at the onset of their entanglement, and their minimum and maximum entanglement duration (d), minimum swimming distance while entangled (km), and average fold increase in drag from their entangling gear.

Catalog number	Gear number	Age at entanglement	Length (cm)	Weight (kg)	Entanglement duration (minimum–maximum; d)	Minimum swim distance while entangled (km)	Mean (SD) fold increase in drag
1102	J060801	21	1,435	40,416	100–3,328	5,504	1.05 (0.01)
1427	J071202	18	1,413	35,095	5–487	962	1.22 (0.04)
2030	J051099	12	1,357	24,453	163–769	1,839	1.61 (0.12)
2212	J091298	5	1,235	12,037	1–23	10	3.07 (0.42)
2212	J072498	6	1,260	13,811	332–346	492	1.19 (0.08)
2223	J081800	8	1,300	17,359	263–300	2,524	1.20 (0.04)
2710	J072199	3	1,164	8,490	68–397	119	1.39 (0.08)
3107	J070602	1	1,011	4,943	57–297	128	1.38 (0.11)
3294	J120808	6	1,260	13,811	11–293	53	1.47 (0.11)
3311	J011409	7	1,282	15,585	51–2,510	5,232	1.71 (0.20)
3314	J120604	2	1,108	6,717	25–98	659	1.92 (0.23)
3420	J013109	5	1,235	12,038	12–352	1,506	1.11 (0.01)
3445	J120305	2	1,108	6,717	9–2,459	1,213	1.69 (0.19)
3610	J092706	3	1,164	8,490	119–435	2,619	1.06 (0.02)
3714	J020709	2	1,108	6,717	5–64	169	1.07 (0.02)

was estimated from body length as presented in (Fortune *et al.* 2012):[2]

$$d_{\max} = 0/21l + 38.63, \tag{7}$$

and diameter (d_j; cm) at multiple (j) stations along the body from width-to-length ratio of mesomorphic right whales (van der Hoop *et al.* 2013*b*). Although length, weight, and width data are available for some of these cases at the time of death, postmortem body dimensions would reflect body shape following the impact of the course of an entanglement, rather than at its onset.

The total drag on each whale (DW) is calculated as

$$DW = Fgk, \tag{8}$$

where g and k are drag augmentation factors. The appendage drag factor $g = 1.3$ accounts for increases in interference, frictional and pressure drag by ~30% from fins and flukes (Fish and Rohr 1999). The body oscillation drag factor k accounts for increases in frontal area and pressure drag due to the oscillation of the flukes and body during active swimming (Fish and Rohr 1999). Due to uncertainties on the magnitude of anterior oscillation, $k = 1.5$ with a range of 1.35–1.65 (± 10%). Compared to van der Hoop *et al*. (2013*b*), the effect of surface wave drag (γ) is not included, as recent data suggest that whales show variable and opposite responses in submergence due to drag and buoyant forces associated with entanglement (van der Hoop *et al*., unpublished data).

Case-specific drag measurements were added to each individual whale's body drag, as in van der Hoop *et al.* (2013*b*). Briefly, for all n cases, the interference drag coefficient was calculated for all j gear attachment points ($C_{dI_{n,j}}$)

$$C_{dI_{n,j}} = \left(\frac{h_j}{\delta_j}\right)^{1/3}, \tag{9}$$

where h is the height (m) of the gear and δ is the boundary layer thickness (m) at all j gear attachment locations (proportion of body length; l_j), calculated as

$$\delta_j = \left(\frac{d_{\max}}{d_j}\right)0.02l_j, \tag{10}$$

Total interference drag for each n case is then the sum of interference drag at all j gear attachment points:

$$DI_n = \sum_j DI_{n,j} = \sum_j \frac{1}{2}\rho U^2\ A_{n,j}CDI_{n,j}. \tag{11}$$

Compared to van der Hoop *et al.* (2013*b*), the shielding effects of the whale's body (~12 m) are ignored here, as similar shielding likely occurred behind the tow fish and

[2]Personal communication from Sarah Fortune, Marine Mammal Research Unit, Institute for Oceans and Fisheries, University of British Columbia, Vancouver, British Columbia V6T 1Z4, Canada, 29 September 2015. There is an error in the equation printed in Fortune *et al*. (2012), where the reported values of slope and intercept are reversed. Equation 7 is the correct equation.

in the wake of the vessel (18 m). The total drag for each entangled whale (DT_n:N) is then

$$DT_n = DW_n + DG_n + DI_n, \tag{12}$$

where DG_n (N) is the drag on the entangling gear measured from the tensiometer at all depths and speeds, fitted with power functions by nonlinear least squares. Lower and upper estimates of DT_n are obtained by incorporating the 95% prediction intervals of DG_n and calculating DI_n with $C_{dI} \pm 10\%$ (Fig. 3).

Propulsive power (P_p, W) is computed as

$$P_p = \frac{DT_n U}{\eta} \tag{13}$$

where η is an efficiency coefficient of 0.15 (Fish and Rohr 1999, van der Hoop *et al.* 2013*b*).

Because individual whales vary in their dimensions, gear varies in the amount of measured drag and estimated interference drag, and measured drag and interference drag do not necessarily correlate, the contributions of each drag component (*DW, DG, DI*) to *DT* were calculated.

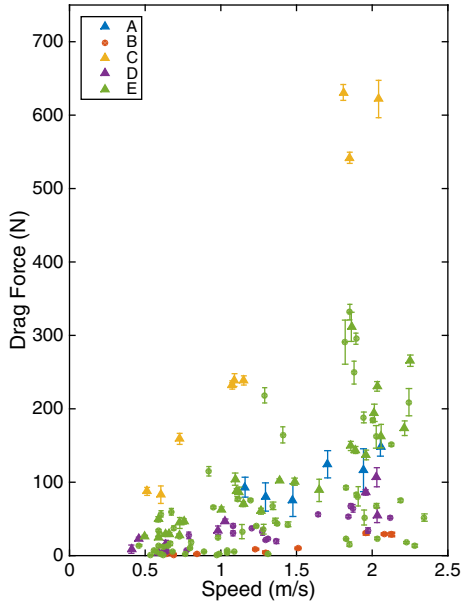

Figure 3. Drag on sets of entangling fishing gear is highly variable. Measured drag force (N) of 15 sets of fishing gear (colored by cluster; see text, Fig. 4) removed from entangled right whales and a satellite telemetry buoy used to track entangled whales (blue, cluster A) towed across a range of speeds, averaged over depths of 0, 3, and 6 m. Gear sets made up of line only are represented as circles, and gear sets with floats or buoys as triangles.

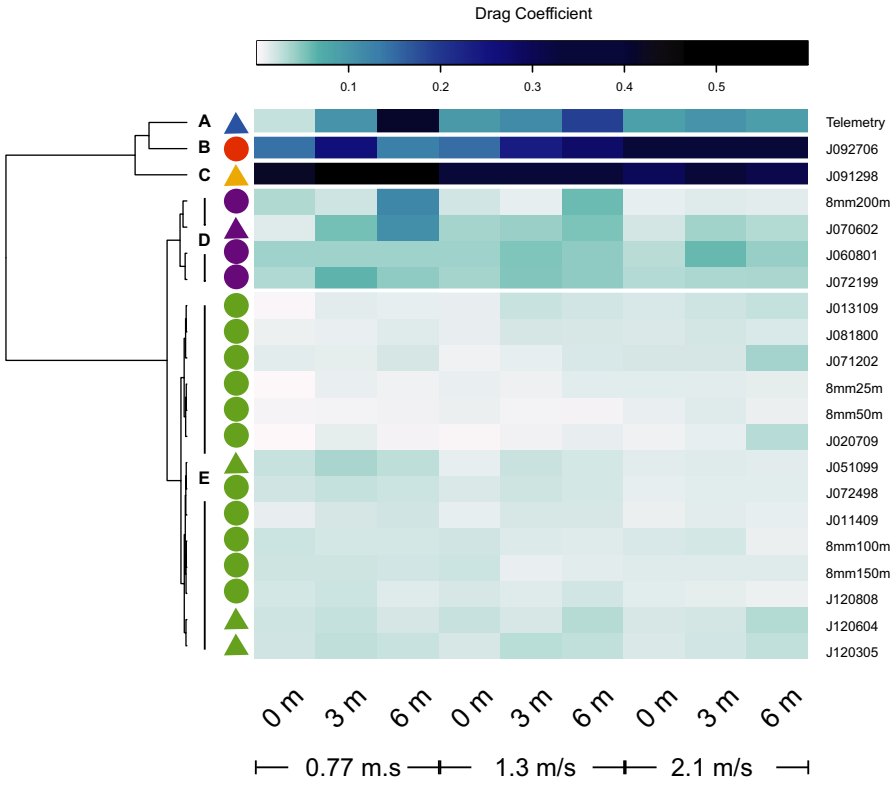

Figure 4. Hierarchical clustering separates entangling fishing gear sets into five groups. Drag coefficients of 21 fishing gear configurations measured at different depths and speeds, separated by row-wise hierarchical minimal variance Ward's clustering. Five clusters (A through E) are identified by separate colors. Gear sets made up of line only are represented as circles, and gear sets with floats or buoys as triangles.

Results

Entangling Gear Description

Fifteen sets of fishing gear removed from entangled right whales were used in this study (Appendix S2). Ten sets were made up of line only, while five sets included floats or buoys; one of these five included a two-brick lobster trap. Identified gear types were trap/pot (n = 6), longline (n = 1), gill net (n = 1), and unidentified fixed gear (n = 1); six sets were unable to be identified. Gear sets with floating rope only (n = 11), sinking rope only (n = 1), and both floating and sinking rope (n = 3) were recovered. The majority of lines were twisted three-strand polypropylene, 0.8–1.6 cm (5/16" –5/8") in diameter.

There is considerable variation in the magnitude of drag forces measured from entangling fishing gear (Fig. 3). At the lowest tested speeds (~0.5 m/s) the drag measured on all 21 gear configurations ranged 0 to 83 N; at the highest tested speeds (~2 m/s), drag forces ranged 18 to 630 N. Coefficients of variation ranged 0.0132 to

10.08 across all measured depths and speeds for all gear sets. The median CV was 0.089; high CVs occurred at the lowest speeds, because CV approaches infinity as mean measured drag values approach zero. Drag coefficients (C_d) range from $9.2 \times 10^{-3} \pm 0.0029$ to 0.45 ± 0.13 across gear configurations (Fig. 4, S2). The mean±SD power relating drag and speed across all gear sets ($n = 21$) was 1.43 ± 0.52, less than the expected theoretical drag $\approx$ speed^2 relationship.

Hierarchical cluster analysis separated gear configurations into five groups based on drag coefficient and its response to changes in depth and speed (Fig. 4). The telemetry buoy, a two-brick lobster trap (J091298) and an extremely short gear configuration (J092706) cluster independently from the rest of the gear sets towed. A small cluster of four gear configurations is also apparent. The presence of buoys, traps, or floats on the gear sets is not directly related to clustering, as gear sets with these features occur in many clusters (Fig. 4). Further, the drag coefficients, lengths, and weights of gear sets with buoys, traps, or floats do not fall at the extremes of those within each cluster. Across speeds of 0.5–2.5 m/s, the Froude number (Fn) of floats on three gear sets (Appendix S1, Fig. S3) ranged 0.16–0.95 and 0.27–1.34 for the telemetry buoy.

Depth and speed differentially affect the drag coefficients of gear sets in these five clusters (Fig. S2). Drag coefficients in clusters A, B, D, and E decrease with increasing speed, whereas the drag coefficient of cluster C (J092706) increases with speed. Drag coefficients of gear in clusters A and D increase with depth. In clusters C and E, drag coefficients are lower at greater depth at the lowest speeds, but become greatest at the greatest depth and speed. The gear in cluster B shows multiple interacting effects of drag and speed on drag coefficient.

Percent differences in drag coefficient range 22%–81% (median 37%) with depth, and 18%–74% (median 48%) with speed. For 14/21 cases, occurring in all gear clusters, drag coefficients vary more with speed than with depth. There is no pattern for whether gear sets with floats are more affected by depth or by speed.

Linear models suggest that mean drag forces (N) measured over all combinations of depths and speeds can be predicted from dry weight (kg), as Drag = $5.9 + 9.1 \times$ Weight ($R^2 = 0.983$, RMSE = 8.63; $F_{1,12} = 680$, $P < 0.0001$; Fig. 5A). More practically, drag can also be predicted from the length of the gear (m), as:

$$\text{Drag} = 8.67 + 0.47 \times \text{Length} + 39.26 \times \text{Float} + 0.01 \times \text{Length} \times \text{Float}, \quad (14)$$

where Float is a binary variable depending on whether the gear set includes floats or buoys ($R^2 = 0.812$, RMSE = 21.2; $F_{3,16} = 23.1$, $P < 0.0001$; Fig. 5B). There is no detectable difference in the slopes of float *vs.* nonfloat gear ($F_{1,16} = 0.0011$, $P = 0.9729$), but note the much higher intercept for gear with floats. The lobster trap (J091298) was deemed an outlier and was not used in weight or length regression analyses based on Cook's D = 1.2 and 1.64 ($\gg 4/n$ in both cases), respectively.

Effect of Partial Gear Removal

To understand the incremental gain in removing entangled gear to reduce parasitic gear drag and the energetic impact on an individual, a piece of 8 mm diameter polypropylene line was shortened from 200 m to 25 m. By comparing drag measurements at the surface across a range of speeds for each length of line, the incremental effect of line length on parasitic drag was determined. As expected, the magnitude of the drag force at a given speed decreases with shorter lengths of line (Fig. 6A).

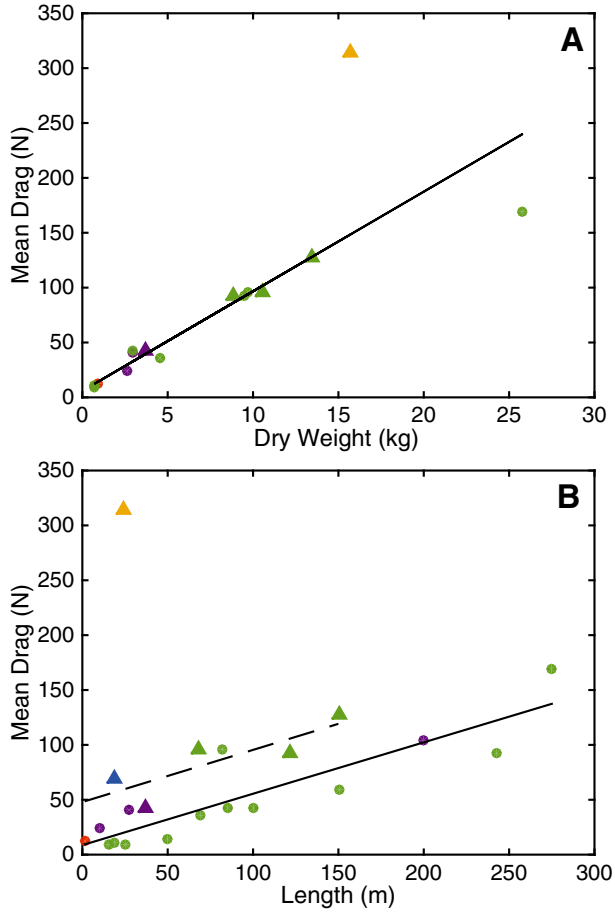

Figure 5. Mean drag (N) measured across speeds and depths can be predicted by the dry weight (kg; A) or length (m; B) of a gear set. Colors represent different groupings of gear identified by hierarchical clustering (see text). Gear sets made up of line only are represented as circles, and gear sets with floats or buoys as triangles. Black lines illustrate linear model fits of mean drag and (A) weight; and (B) length, with the presence of floats (dashed line) as a categorical covariate. See text for equations.

Similarly, drag coefficients systematically decrease with towed line length, from 0.041 ± 0.039 at 200 m to 0.011 ± 0.0043 at 25 m (Fig. S4). Comparing drag estimates from fitted curves indicates that considerable reductions in parasitic drag can be achieved by reducing the length of a set of entangling gear (Fig. 6B, C). For example, a 200 m long line cut to 50 m results in an 83.4% ± 6.0% reduction in drag across speeds (Fig. 6B); removing 75% of a line's original length reduces parasitic gear drag by 85.0% ± 7.4% across speeds (Fig. 6C). The greatest gains in parasitic drag reduction are achieved at the lowest swimming speeds, where 75% removal yields a 93.8% ± 3.3% parasitic drag reduction at 0.5 m/s compared to 78.8% ± 1.0% at 2.00 m/s (Fig. 6C).

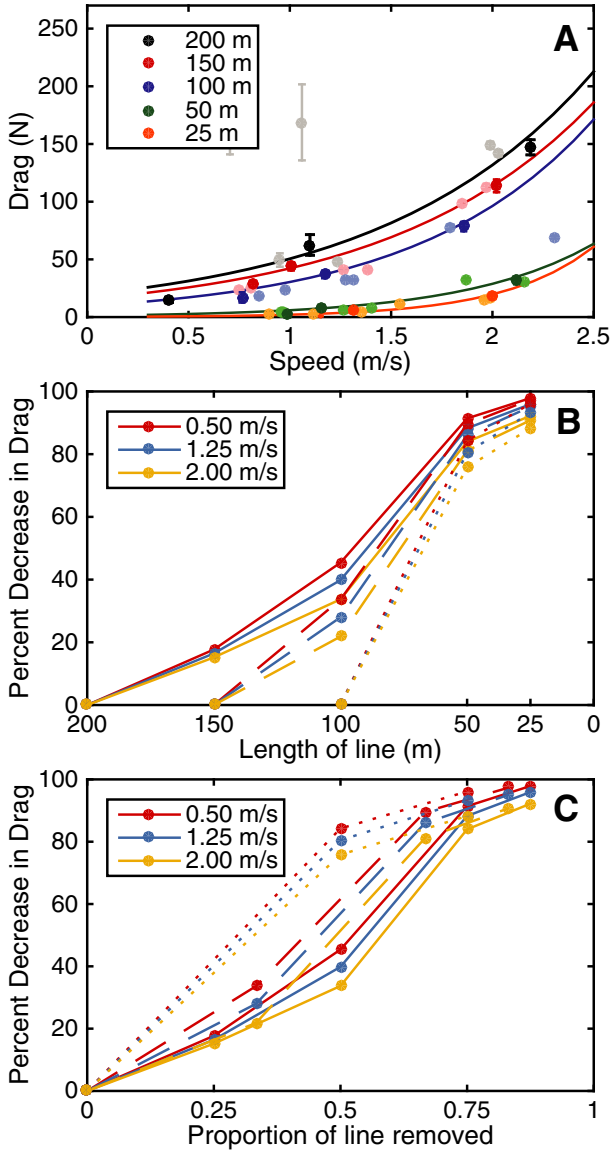

Figure 6. Drag force decreases with towed line length. (A) Measured mean ± SD drag forces (N) with speed (m/s) on different lengths of 8 mm diameter polypropylene fishing rope towed at the surface (darker colors) and at 3 and 6 m depth (lighter colors). Lines represent power functions fit to surface drag values. (B) Percent decrease in drag as a line is shortened from 200 m (solid line), 150 m (dashed line), 100 m (dotted line), and 50 m (no line) to its new length (*x*-axis) at speeds of 0.50, 1.25 and 2.00 m/s. (C) Percent decrease in drag with the proportion of line removed from 200 m (solid line), 150 m (dashed line), 100 m (dotted line), and 50 m (no line) to its new length (*x*-axis) at speeds of 0.50, 1.25, and 2.00 m/s. For example: trimming a 200 m line to 150 m, equivalent to having removed 0.25 of the line, results in a 14% decrease in drag at 2.00 m/s.

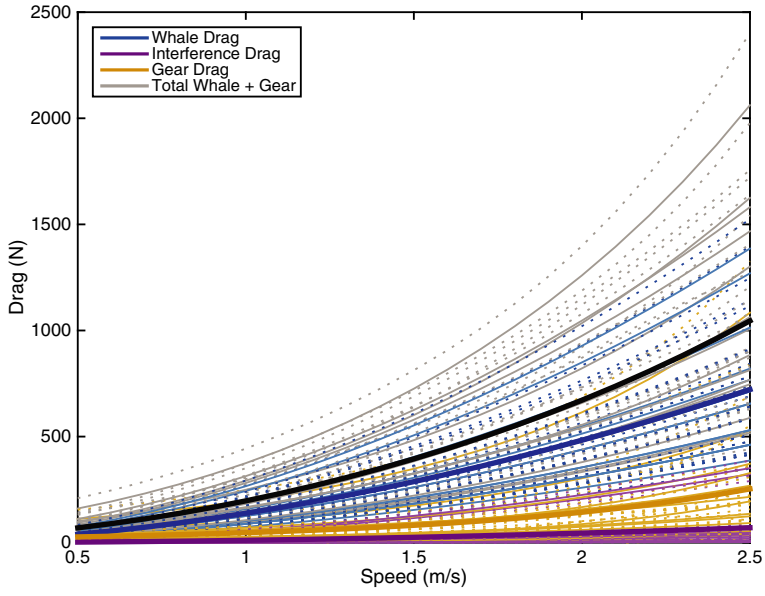

Figure 7. Estimated total body drag on entangled and nonentangled whales and entangling gears. Drag force (N) of 15 individual right whales when not entangled (blue), their entangling fishing gear (yellow), interference drag from the entangling gear (purple), and when entangled in these fishing gear (black). Thicker lines represent means.

Entangled Whale Drag

Average drag on nonentangled whales ranged between 40 ± 16 and 721 ± 297 N across speeds of 0.5–2.5 m/s (Fig. 7). Modeled drag coefficients for nonentangled whales ranged 0.0029–0.0040, similar to as modeled in van der Hoop *et al.* (2013*b*; 0.0028–0.0037) and measured during traveling (0.0036–0.0052) and foraging (0.0091–0.024; McGregor 2010). At the upper 95% CI swimming speed of nonentangled right whales of 1.23 m/s (Baumgartner and Mate 2005), the average drag for these 15 individuals is 193 ± 79 N. When entangled in their specific gear configurations at 1.23 m/s, drag is significantly increased to 268 ± 115 N (paired *t*-test; t_{14}, = 3.35, P = 0.0031), by 1.42 ± 0.46 fold (Fig. 8). The mean increase in drag from entanglement across speeds, is 1.47 ± 0.52 fold, with a maximum of 3.07 ± 0.42 fold, *i.e.*, three times over the nonentangled condition (Fig. 7).

Drag from entangling fishing gear is 0.35 ± 0.38 of the drag on the whale's body across speeds (Fig. 8). Drag from entangling gear approaches or exceeds the magnitude of drag from the whale's body alone in four cases, primarily at the lowest speeds (0.5–0.7 m/s). Additionally, gear drag is 1.78–3.45 fold greater than whale body drag across speeds for case J091298. Estimated interference drag (*DI*) is variable among all gear sets, ranging from 1.3 N to 147.1 N, contributing on average 39% to the total drag from entangling gear (*DG* + *DI*; Fig. 8).

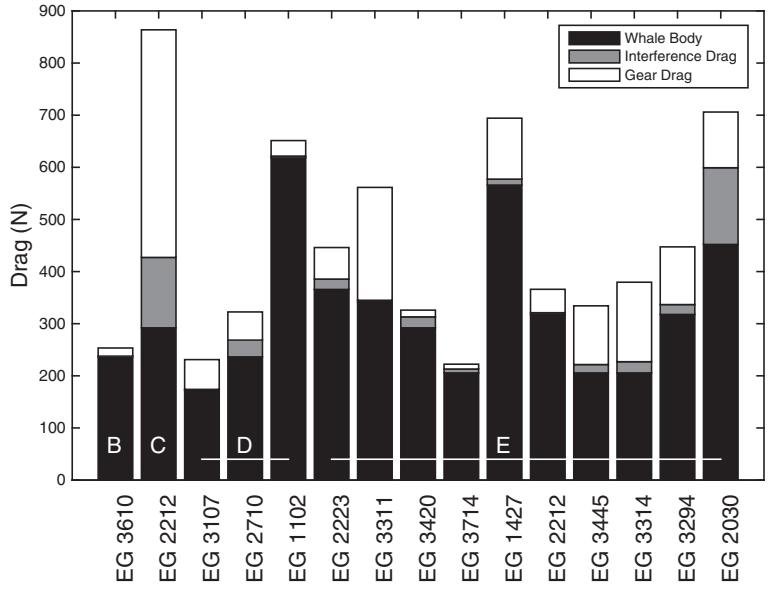

Figure 8. Contributions of whale body drag, estimated interference drag, and measured drag on entangling gear for 15 entangled North Atlantic right whales (identified by EG code). Letters identify gear type clusters (see text; note cluster A is not attributed to a specific right whale case).

Discussion

Entanglement in fishing gear contributes significant mortality to many large whale species (van der Hoop *et al.* 2013*a*). The fatality of an entanglement, its time course, candidacy for disentanglement, and sublethal effects are all complex aspects of the same incident, largely related to the amount of gear involved and its configuration on the animal. This study sought to measure drag on sets of fishing gear that have entangled or are similar to those entangling North Atlantic right whales, describe differences in their responses to drag and speed, and put these differences in the context of the whales that the gear entangled. The average drag forces and coefficients of measured gear sets range up to two and four orders of magnitude. Such variation is expected, as the cases selected for this experiment represent the great diversity of sizes, shapes and types of fishing gear entangling whales (Johnson *et al.* 2005). Minimum values are therefore especially notable: seemingly small entanglements (short pieces of line, small floats) can still impart significant drag.

Estimated drag coefficients can be compared with those reported elsewhere. The highest drag coefficient of the gear set with a lobster trap measured in this study was 0.69 (6.4 m, 0.51 m/s, $Re = 3 \times 10^7$), considerably lower than the 2.3 reported by (Budiman *et al.* 2004) for a similar size crab trap at low flow speeds (0.1–0.5 m/s) and Reynolds number ($Re = 1.0 \times 10^3 - 6.7 \times 10^3$). This disparity is likely due to different experimental setups, where a large amount of low drag-coefficient rope was attached to the pot in this study. Rope drag coefficients range from 0.12 to 1.30, depending on material and degree of wear, but primarily increase with the angle between rope and flow direction (Fridman 1986). In this study, drag coefficients

increased with depth on average (Fig. 4, S2), likely due to the increase in frontal area when lines are buoyed to the water surface (Fig. 1, orange line); those that did not follow this trend may have been neutrally buoyant, trailing at the same depth instead of being taut to the surface. Buoyancy will greatly affect the shape of gear underwater (Baldwin and Pickett 2009), as will the tension on the line, which increases with ship speed. These considerations constrain the application of standard formulae to estimate the effect of depth on drag of unmeasured gear sets.

Measured drag forces are also comparable to those in other studies. van der Hoop *et al.* (2013*b*) present a similar range of drag measurements for a 25 m line-only configuration (3–70 N across 0.77–2.8 m/s), which increased by ~72% with the addition of two 42–45 cm spherical buoys. Bullet-style lobster buoys on short (0.5 m) tethers can have measured drag as low as 22 N at 2 m/s, while a standard, single double-brick lobster pot may add 222 N (Woodward *et al.* 2006). Gear configurations with multiple floats and buoys, as observed in five cases in this study, can have especially high drag: a single 40" circumference Scanmarin float with two 6" × 4" buoys on a 183 m line can be as high as 1,245 N at the same speeds (Salvador and Kenney 2002). These measured differences in drag with the addition of accessory items support the use of separate equations (with and without floats) when estimating drag from gear set length (Fig. 5B).

Drag measurements were performed in the wake of a vessel, which may lead to differences in the absolute values of drag as experienced behind a whale. Although speed through water was calculated from current speeds, the ship's wake may have reduced flow speeds experienced by the gear, leading to underestimates of C_d. Measurements of drag from the gear sets therefore ignore the shielding effects of the vessel. When combining with a theoretical whale, no shielding effects are added, as it is assumed that the vessel (R/V *Tioga* = 18 m) likely imparts similar shielding effects as a right whale's body (10.1–14.3 m in this study). Turbulence from vortices from the ship's propellers, and conversely, the whale's locomotory movements, could additionally generate transverse forces which would interact with gear and its features in an unpredictable manner based on buoyancy, depth, *etc*. Mean gear drag measurements in this study were taken from the 30 s period with the lowest variance in drag to account for potential variability from small changes in hydrodynamics. The drag forces measured on the gear in this study were all performed in the same regime, which at least allows for within-study comparisons to be made.

Mean drag on a set of entangling gear can be predicted from the dry weight or length of the gear (Fig. 5, Eq. 14). This allows for the average drag forces experienced by an entangled animal to be estimated at the time of its detection. Floats, including the telemetry buoy, add 39 N of drag. Although floats do not drive the separation of clusters in drag coefficient, it has a significant effect on the drag-length relationship. Floats on measured fishing gear have a Froude number in the range of 0.16–0.95, while the telemetry buoy has a higher *Fn*, 0.27–1.34, over the 0.5–2.5 m/s speed range (Fig. S3). Especially at routine right whale swimming speeds (1–1.5 m/s) *Fn* is on average 0.43 ± 0.06 for fishing gear or 0.64 ± 0.08 for the telemetry buoy. Wave drag is greatest at *Fn* = 0.5 (Lighthill 1978). The wave drag from these gear sets is a component of the total resistance measured by the tensiometer (*DG*). Calculating and comparing *Fn* shows that gear sets with floats have high wave drag, especially at average swimming speeds of right whales.

This study estimates the increase in drag and propulsive power experienced by the right whales entangled by each gear set (Fig. 7, 8), based on gear-specific measurements and individual-specific morphometrics. Inter- and intraspecific body shape

changes affect drag and buoyant forces on a whale's body (*e.g.*, Woodward 2006, Nousek-McGregor *et al.* 2013). While individual variation in body shape at the onset of entanglement is included, the change in body condition that typically occurs through the course of the entanglement as energy is depleted is ignored (van der Hoop, unpublished data; Ahlborn *et al.* 2009; Barratclough *et al.* 2014). Almost all (49/50; Robbins *et al.* 2015) photo-identified entangled right whales are in good body condition at their last sighting prior to entanglement detection. The rate of deterioration in body condition is a function of a number of known factors, *e.g.*, increased drag and power, but is highly dependent on a number of unknowns, including the location and feeding status of each individual at the time of onset.

Factors such as interference drag and the point(s) of gear attachment have been estimated, as they alter boundary layer flow. Entangling gear that is raised off the body more than 0.001 × body length (*e.g.*, a float in the mouth, a gill net across the back) can produce serious disturbance to fluid flow (Jacobs 1934). The relative contributions of interference drag to total drag (Fig. 8) are highly variable across gear sets, and are also influenced by the point of attachment: forward of the maximum-thickness position, flow-disturbance is greatest, having similar effects to air brakes (Jacobs 1934).

There are at least two broad factors contributing to the lethality of an entanglement configuration: the presence or absence of wraps of body parts and drag (at those body parts and to the whale as a whole). This study addresses some of the issues surrounding one of those factors: drag. By lessening the energy cost of swimming as well as the tension on entangled body parts, reducing drag certainly could benefit a whale with 300 m of line trapped in its baleen (Fig. 2A); however, drag reduction is unlikely to save a whale with a rostrum or body wrap with only 10 m of line trailing (Fig. 2B), as trained responders need at least some trailing line to address body wraps in follow-up disentanglement attempts. Reducing drag, as seen in these results, can help in some whale entanglement cases, but will not resolve those that involve wraps of body parts (*e.g.*, Eg 3346 in Moore *et al.* 2013).

This study reinforces the current practice of reducing trailing gear to roughly a whale's body length prior to adding the telemetry buoy for subsequent disentanglement efforts, which ultimately enhance survival (Robbins *et al.* 2015). While this practice originated with the desire to reduce the chance that trailing line would re-entangle the whale or other gear, these results highlight the practice of minimizing trailing line from an entirely different perspective. Responders can be urged to reduce drag to a "reasonable" minimum while allowing them enough access to the other elements of the entanglement (*e.g.*, wraps of body parts). Simply cutting off all trailing gear is not going to solve an entanglement, especially if doing so reduces access to the remaining entanglement configuration. Drag can also be useful for whales to disentangle themselves, *e.g.*, when drag on the trailing end of gear is sufficient to pull rope from baleen (Cavatorta *et al.* 2005). As scarring rates in many different whale populations (Neilson *et al.* 2009, Knowlton *et al.* 2012, Robbins 2012) greatly exceed entanglement mortalities, reported entanglements, and sightings of animals with gear, many whales are able to shed gear on their own.

Gear drag contributes to the immediate sublethal effects of entanglement: direct injury and physiological disturbances, such as stress and metabolic responses (Wilson *et al.* 2014). Greater drag loading leads to more severe entanglement-related injuries, increasing both the depth and length of furrows (Woodward *et al.* 2006). Epidermal penetration occurs when tensions exceed regional tissue compliance (Winn *et al.* 2008): nine and six (60% and 40%) of the 15 right whale cases presented here exceed

tensions that create 0.27 and 0.40 cm deep furrows, respectively, in right whale peduncles over the equivalent of five days of swimming at 2 m/s (Woodward *et al.* 2006). These injuries were modeled over a much shorter duration than the 15 cases presented here (Table 2). Consistent drag on gear cutting into the tissues has led to near (*e.g.*, cases VAQS2005-1008Eg [Eg 2301] and MH02-736-Eg [Eg 3107] in Moore *et al.* 2013) and complete (Urban *et al.* 2004, IWC 2011) pectoral and caudal fin amputations.

Physiological responses to stress, injury, wound repair, and metabolic disturbance due to drag loading and altered swimming behaviors all interact (Hunt *et al.* 2006, Archie 2013); health impairment (Pettis *et al.* 2004, Robbins *et al.* 2015) and energetic costs can begin to be estimated in terms of cost to an individual. The 15 entanglements studied here lead to significant increases in drag and propulsive power output in right whales (Fig. 7). When swimming at 2.0 m/s, nonentangled whales expend on average 2.3% ± 0.1% and 9.4% ± 0.2% of their estimated maximal and submaximal force outputs, respectively (Arthur *et al.* 2015). When entangled, these force outputs increase to 3.3% ± 1.0% and 13.2% ± 4.5%. Sustained over long periods (mean ± SD minimum 81 ± 100 and maximum 810 ± 1,044 d in these 15 cases; Table 2), such increases have the potential to lead to significant alteration to time and energy budgets and reductions in body condition (Feldkamp 1985). Disentanglement has shown to increase survival in life-threatening entanglement cases, although health impacts are most predictive of subsequent survival (Robbins *et al.* 2015). Despite concerted and dedicated efforts to remove or reduce the impacts of entangling gear, postdisentanglement mortality occasionally occurs, likely due to significant reductions in heath and body condition prior to entanglement detection or response (Moore *et al.* 2010, 2012). Additionally, body condition is a major contributor to reproductive success in many mammals, including right whales (Cassoff *et al.* 2011, Moore *et al.* 2013, van der Hoop *et al.* 2013*b*). It is conceivable that energy reserves may be sufficiently affected by chronic gear drag so as to limit future individual reproductive success. Further analysis of the impact of fishing gear entanglement drag on energy balance is therefore warranted. These hidden, sublethal costs of entanglement are not currently considered in the annual North Atlantic right whale stock assessment reports, which form the basis of the U.S. Government management of this endangered species, but are likely a significant contributor to the variability in annual right whale recruitment.

Conclusions

Entanglement in fishing gear remains a significant issue for marine animal species worldwide (Hofmeyr *et al.* 2006, Moore *et al.* 2009, Moore and Barco 2013, van der Hoop *et al.* 2013*a*). While mortality is the simplest indicator of a negative entanglement outcome, the subtler sublethal effects in the form of stress response, metabolic disturbance, and behavioral impairment can and should be considered (Wilson *et al.* 2014), especially in cetaceans, where mortality detection probabilities are remarkably low (Williams *et al.* 2011, Wells *et al.* 2014). The amount of drag imposed from entangling gear is a factor in defining entanglement cases as "Serious Injury" for the purposes of the U.S. Marine Mammal Protection Act and/or U.S. Endangered Species Act (NOAA 2008). The ability to determine gear drag from length (which can be estimated from photos) and the drag reductions of gear removal enables the prediction of a drag scenario of free-swimming entangled individual when detected, to be applied when planning disentanglement response and in case-by-case evaluations of

serious injuries and stock assessment reports for U.S. Federally mandated endangered species conservation.

Acknowledgments

The authors would like to thank the crew of the R/V *Tioga* for assistance, necropsy responders and members of the ALWDN for their collection and cataloging of entangling fishing gear, the North Atlantic Right Whale Consortium for data access, and those members of stranding and disentanglement crews who contribute to the database. Entanglement responses were conducted under NOAA MMHSRP permits 932-1489 and 932-1905 and appropriate Fisheries and Oceans Canada licenses.

This work was supported by grants from the Herrington-Fitch Family Foundation, the M.S. Worthington Foundation, and the Cooperative Institute for the North Atlantic Region [CINAR; NA14OAR4320158] to MJM and JvdH. JvdH was supported by a Postgraduate Scholarship from the Natural Sciences and Engineering Research Council of Canada, and an MIT Martin Family for Sustainability Fellowship.

JvdH and MJM developed concepts; JK, SL, JS provided historical data and gear; JvdH, DM, MJM performed fieldwork; JvdH processed and analyzed the data; PC provided statistical guidance; JvdH, PC, JK, SL, DM, JS, MJM contributed to the manuscript.

Literature Cited

Ahlborn, B. K., R. W. Blake and K. H. S. Chan. 2009. Optimal fineness ratio for minimum drag in large whales. Canadian Journal of Zoology 87:124–131.

Archie, E. A. 2013. Wound healing in the wild: Stress, sociality, and energetic costs affect wound healing in natural populations. Parasite Immunology 35:374–385.

Arthur, L. H., W. A. Mclellan, M. A. Piscitelli, *et al*. 2015. Estimating maximal force output of cetaceans using axial locomotor muscle morphology. Marine Mammal Science. doi:10.1111/mms.12230.

Baldwin, K., and T. Pickett. 2009. The time tension line cutter evaluation: Fishermen pilot study and controlled experiments. Final report for NOAA Contract NA08NMF4270419. 101 pp. Available at http://www.greateratlantic.fisheries.noaa.gov/whaletrp/trt/meetings/Mid-Atlantic_Southeast_ALWTRT_Materials/UNH Report_time tension line cutter.pdf.

Barco, S. G., L. R. D'Eri, B. L. Woodward, J. P. Winn and D. S. Rotstein. 2010. Spectra fishing twine entanglement of a bottlenose dolphin: A case study and experimental modeling. Marine Pollution Bulletin 60:1477–1481.

Barratclough, A., P. D. Jepson, P. K. Hamilton, C. A. Miller, K. Wilson and M. J. Moore. 2014. How much does a swimming, underweight, entangled right whale (*Eubalaena glacialis*) weigh? Calculating the weight at sea, to facilitate accurate dosing of sedatives to enable disentanglement. Marine Mammal Science 30:1589–1599.

Barron, D. G., J. D. Brawn and P. J. Weatherhead. 2010. Meta-analysis of transmitter effects on avian behaviour and ecology. Methods in Ecology and Evolution 1:180–187.

Batchelor, G. K. 2000. An introduction to fluid dynamics. Cambridge University Press, Cambridge, U.K..

Baumgartner, M. F., and B. R. Mate. 2005. Summer and fall habitat of North Atlantic right whales (*Eubalaena glacialis*) inferred from satellite telemetry. Canadian Journal of Fisheries and Aquatic Sciences 62:527–543.

Budiman, J., S. Fuwa and K. Ebata. 2004. Fundamental studies on the hydrodynamic resistance of small pot traps. Fisheries Science 70:952–959.

Cassoff, R. M., K. M. Moore, W. A. Mclellan, S. G. Barco, D. S. Rotstein and M. J. Moore. 2011. Lethal entanglement in baleen whales. Diseases of Aquatic Organisms 96:175–185.

Cavatorta, D., V. Starczak, K. E. Prada and M. J. Moore. 2005. A note on the friction of different ropes in right whale (*Eubalaena glacialis*) baleen: An entanglement model. Journal of Cetacean Research and Management 7:39–42.

Feldkamp, S. D. 1985. The effects of net entanglement on the drag and power output of a California sea lion, *Zalophus californianus*. Fishery Bulletin 83:692–695.

Feldkamp, S. D., D. P. Costa and G. K. Dekrey. 1988. Energetic and behavioral effects of net entanglement on juvenile northern fur seals, *Callorhinus ursinus*. Fishery Bulletin 87:85–94.

Fish, F. E. 1993. Power output and propulsive efficiency of swimming bottlenose dolphins (*Tursiops truncatus*). Journal of Experimental Biology 185:179–193.

Fish, F. E., and J. J. Rohr. 1999. Review of dolphin hydrodynamics and swimming performance. U.S Navy SPAWAR Systems Center, San Diego, CA 193 pp.

Fortune, S. M. E., A. W. Trites, W. L. Perryman, M. J. Moore, H. M. Pettis and M. S. Lynn. 2012. Growth and rapid early development of North Atlantic right whales (*Eubalaena glacialis*). Journal of Mammalogy 93:1342–1354.

Fowler, C. W. 1987. Marine debris and northern fur seals: A case study. Marine Pollution Bulletin 18:326–335.

Fridman, A. L. 1986. Calculations for fishing gear designs. Fishing News Books, Farhnam, Surrey, U.K, FAO fishing manuals.

Fridman, A. L., and A. V. Dvernik. 1973. Development of a method for the calculation of the resistance of a trawl net. Fischerei Forschung 11:7–13.

Hofmeyr, G. J., M. N. Bester, S. P. Kirkman, C. Lydersen and K. M. Kovacs. 2006. Entanglement of Antarctic fur seals at Bouvetoya, Southern Ocean. Marine Pollution Bulletin 52:1077–1080.

Hunt, K. E., R. M. Rolland, S. D. Kraus and S. K. Wasser. 2006. Analysis of fecal glucocorticoids in the North Atlantic right whale (*Eubalaena glacialis*). General and Comparative Endocrinology 148:260–272.

IWC. 2011. Report of the second IWC workshop on welfare issues associated with the entanglement of large whales with a focus on entanglement response. IWC/64/WKM&AWI REP1. 28 pp. Available at http://www.icmbio.gov.br/cma/images/stories/CIB__SORP/CIB/Entanglement_report.pdf.

Jacobs, E. N. 1934.Airfoil section characteristics as affected by protuberances. National Advisory Committee for Aeronautics (NACA) Technical Report 446. 16 pp. Available at http://ntrs.nasa.gov/search.jsp?R=19930091520.

Johnson, A., G. Salvador, J. Kenney, J. Robbins, S. Kraus, S. Landry and P. Clapham. 2005. Fishing gear involved in entanglements of right and humpback whales. Marine Mammal Science 21:635–645.

Knowlton, A. R., P. K. Hamilton, M. K. Marx, H. M. Pettis and S. D. Kraus. 2012. Monitoring North Atlantic right whale *Eubalaena glacialis* entanglement rates: A 30 yr retrospective. Marine Ecology Progress Series 466:293–302.

Knowlton, A. R., J. Robbins, S. Landry, H. A. McKenna, S. D. Kraus and T. Werner. 2015. Implications of fishing rope strength on the severity of large whale entanglements. Conservation Biology. doi:10.1111/cobi.12590.

Lighthill, M. J. 1978. Waves in fluid. Cambridge University Press, Cambridge, U.K.

McGregor, A. E. N. 2010. The cost of locomotion in North Atlantic right whales *Eubalaena glacialis*. Ph.D. thesis, Duke University, Durham, NC. 182 pp.

Mendenhall, W., and T. Sincich. 2011. A second course in statistics: Regression analysis. Prentice Hall, Upper Saddle River, NJ.

Moore, E., S. Lyday, J. Roletto, *et al*. 2009. Entanglements of marine mammals and seabirds in central California and the north-west coast of the United States 2001–2005. Marine Pollution Bulletin 58:1045–1051.

Moore, K. T., and S. G. Barco. 2013. Handbook for recognizing, evaluating, and documenting human interaction in stranded cetaceans and pinnipeds. U.S. Department of Commerce, NOAA Technical Memorandum, NOAA-TM-NMFS-SWFSC-510. 102 pp.

Moore, M. J., and J. M. van der Hoop. 2012. The painful side of trap and fixed net fisheries: Chronic entanglement of large whales. Journal of Marine Biology 2012:1–4.

Moore, M. J., A. R. Knowlton, S. D. Kraus, W. A. McLellan and R. K. Bonde. 2004. Morphometry, gross morphology and available histopathology in North Atlantic right whale (*Eubalaena glacialis*) mortalities (1970–2002). Journal of Cetacean Research and Management 6:199–214.

Moore, M. J., A. Bogomolni and R. Bowman, *et al*. 2006. Fatally entangled right whales can die extremely slowly. Oceans'06, MTS/IEEE, Boston, MA 18–21 September 2006. 3 pp.

Moore, M. J., M. Walsh, J. Bailey, *et al*. 2010. Sedation at sea of entangled North Atlantic right whales (*Eubalaena glacialis*) to enhance disentanglement. PLOS ONE 5:e9597.

Moore, M., R. Andrews, T. Austin, *et al*. 2012. Rope trauma, sedation, disentanglement, and monitoring-tag associated lesions in a terminally entangled North Atlantic right whale (*Eubalaena glacialis*). Marine Mammal Science 29:E98–E113.

Moore, M. J., J. M. van der Hoop, S. G. Barco, *et al*. 2013. Criteria and case definitions for serious injury and death of pinnipeds and cetaceans caused by anthropogenic trauma. Diseases of Aquatic Organisms 103:229–264.

Neilson, J. L., J. M. Straley, C. M. Gabriele and S. Hills. 2009. Non-lethal entanglement of humpback whales (*Megaptera novaeangliae*) in fishing gear in northern Southeast Alaska. Journal of Biogeography 36:452–464.

NMFS. 2003. Report of the workshop on large whale disentanglement: Learning from the past and moving towards the future. National Marine Fisheries Service Northeast Regional Office, Boston, MA 68 pp.

NOAA. 2008.Differentiating serious and non-serious injury of marine mammals: Report of the serious injury technical workshop. U.S. Department of Commerce, NOAA Technical Memorandum NMFS-OPR-39. 108 pp.

Nousek-Mcgregor, A. E., C. A. Miller, M. J. Moore and D. P. Nowacek. 2013. Effects of body condition on buoyancy in endangered North Atlantic right whales. Physiological and Biochemical Zoology 87:160–171.

Pettis, H. M., R. M. Rolland, P. K. Hamilton, S. Brault, A. R. Knowlton and S. D. Kraus. 2004. Visual health assessment of North Atlantic right whales (*Eubalaena glacialis*) using photographs. Canadian Journal of Zoology 82:8–19.

Rayleigh, L. 1876. On the resistance of fluids. Philosophical Magazine 5:430–441.

Reid, A. J. 1977. A net drag formula for pelagic nets. Department of Agriculture and Fisheries for Scotland. 14 pp.

Robbins, J. 2012. Scar-based inference into Gulf of Maine humpback whale entanglement: 2010. Report to the National Marine Fisheries Service. Order number EA133F09CN0253. 28 pp.

Robbins, J., A. R. Knowlton and S. Landry. 2015. Apparent survival of North Atlantic right whales after entanglement in fishing gear. Biological Conservation 191:421–427.

Salvador, G., and J. Kenney. 2002. Large whale gear research summary. NOAA Fisheries, Northeast Region, Protected Resources Division Gear Research Team. 159 pp.

Urban, J., V. Flores de Sahagun, M. L. Jones, S. L. Swartz, B. Mate, A. Gomez-Gallardo and M. Guerrero-Ruiz. 2004. Gray whales with loss of flukes adapt and survive. Marine Mammal Science 20:335–338.

van der Hoop, J. M., M. J. Moore, S. G. Barco, *et al*. 2013*a*. Assessment of management to mitigate anthropogenic effects on large whales. Conservation Biology 27:121–133.

van der Hoop, J. M., M. J. Moore, A. Fahlman, *et al*. 2013*b*. Behavioral impacts of disentanglement of a right whale under sedation and the energetic cost of entanglement. Marine Mammal Science 30:282–307.

Warnes, G. R., B. Bolker and L. Bonebakker, *et al*. 2014. gplots: Various R programming tools for plotting data. R package version 2.14.2. Available at http://CRAN.R-project.org/package=gplots.

Webb, P. W. 1975. Hydrodynamics and energetics of fish propulsion. Bulletin of the Fisheries Research Board of Canada 190:1–158.

Wegner, N. C., and D. P. Cartamil. 2012. Effects of prolonged entanglement in discarded fishing gear with substantive biofouling on the health and behavior of an adult shortfin mako shark, Isurus oxyrinchus. Marine Pollution Bulletin 64:391–394.

Wells, R. S., J. B. Allen, S. Hofmann, *et al*. 2008. Consequences of injuries on survival and reproduction of common bottlenose dolphins (*Tursiops truncatus*) along the west coast of Florida. Marine Mammal Science 24:774–794.

Wells, R. S., J. B. Allen, G. Lovewell, J. Gorzelany, R. E. Delynn, D. A. Fauquier and N. B. Barros. 2014. Carcass-recovery rates for resident bottlenose dolphins in Sarasota Bay, Florida. Marine Mammal Science 31:355–368.

Williams, R., S. Gero, L. Bejder, *et al*. 2011. Underestimating the damage: interpreting cetacean carcass recoveries in the context of the Deepwater Horizon/BP incident. Conservation Letters 4:228–233.

Wilson, S. M., G. D. Raby, N. J. Burnett, S. G. Hinch and S. J. Cooke. 2014. Looking beyond the mortality of bycatch: Sublethal effects of incidental capture on marine animals. Biological Conservation 171:61–72.

Winn, J. P., B. L. Woodward, M. J. Moore, M. L. Peterson and J. G. Riley. 2008. Modeling whale entanglement injuries: An experimental study of tissue compliance, line tension, and draw-length. Marine Mammal Science 24:326–340.

Woodward, B. L. 2006. Locomotory strategies, dive dynamics, and functional morphology of the mysticetes: Using morphometrics, osteology, and Dtag data to compare swim performance in four species of baleen whales. Ph.D. thesis, University of Maine, Orono, ME. 195 pp.

Woodward, B. L., J. P. Winn, M. J. Moore and M. L. Peterson. 2006. Experimental modeling of large whale entanglement injuries. Marine Mammal Science 22:299–310.

Yoshida, K., N. Baba, M. Kiyota, M. Nakajima, Y. Fujimaki and A. Furuta. 1990. Studies of the effects of net fragment entanglement on northern fur seals part 2: Swimming behavior of entangled and nonentangled fur seals. Pages 503–512 *in* R. S. Shomura and M. L. Godfrey, eds. Proceedings of the Second International Conference on Marine Debris, 2–7 April 1989, Honolulu, HI.

Received: 1 May 2015
Accepted: 26 October 2015

Supporting Information

The following supporting information is available for this article online at http://onlinelibrary.wiley.com/doi/10.1111/mms.12292/suppinfo.

Appendix S1. Estimating wetted surface area and Froude number of gear configurations.

Appendix S2. Sets of fishing gear removed from entangled North Atlantic right whales used in this experiment.

Figure S1. Dimensions (A) and in situ photograph (B) of the satellite telemetry buoy used for tracking entangled whales for later disentanglement attempts.

Figure S2. Groups of gear have similar drag coefficients and responses to depth and speed. Average drag coefficients (C_d) of five clusters (A through E; by hierarchical clustering) of 21 sets of fishing gear removed from or similar to those entangling

North Atlantic right whales across speeds, at depths of 0 m (solid black), 3 m (dashed black), and 6 m (dotted black). Gray lines illustrate estimated drag coefficients for all gear within that cluster, from which averages are calculated. Note the difference in the *y*-axis limits for panels A, B, C *vs.* D, E.

Figure S3. Froude number (*Fn*) with speed (m/s) for three sets of fishing gear removed from entangled right whales (J070602, J120305 and J120604) and the satellite telemetry buoy. Colors represent different gear clusters (see text for details). The magnitude of the wave drag effect is shown for a range of *Fn* (relative; see Lighthill 1978).

Figure S4. Changes in drag coefficient with towed line length (A), Reynolds number (*Re*; B), and speed (C).

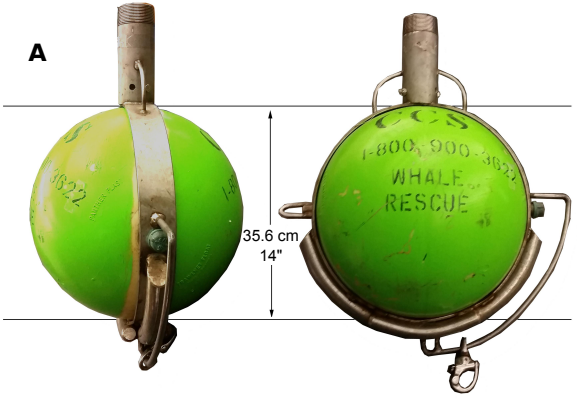

Figure S1. Dimensions (A) and in situ photograph (B) of the satellite telemetry buoy used for tracking entangled whales for later disentanglement attempts.

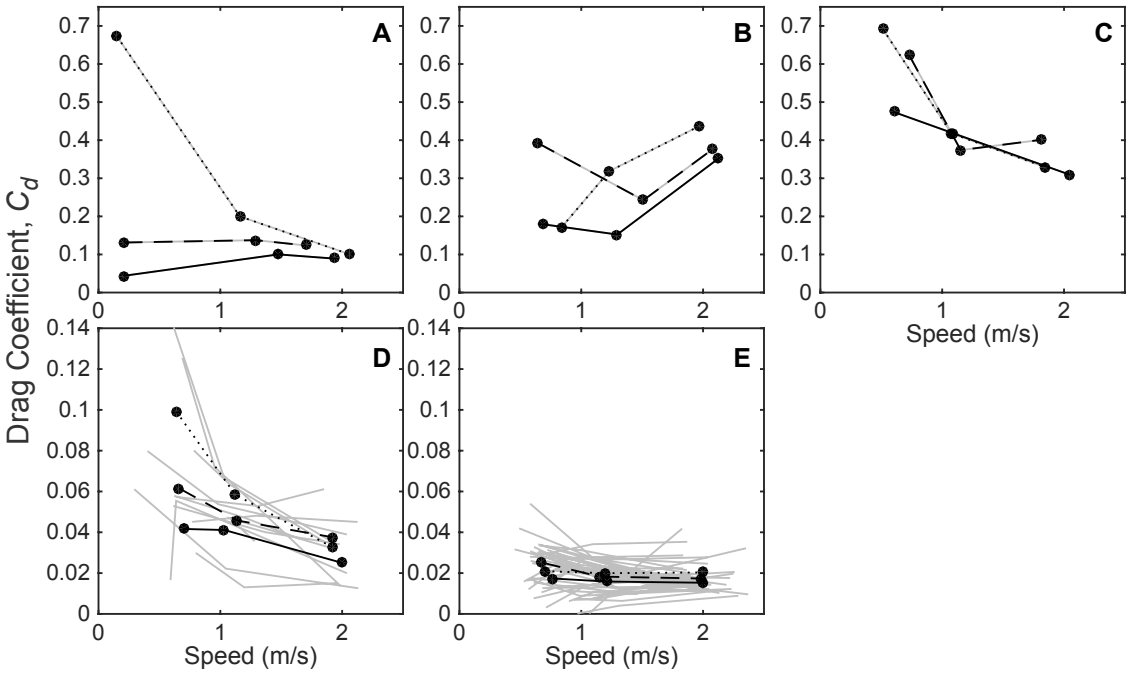

Figure S2. Groups of gear have similar drag coefficients and responses to depth and speed. Average drag coefficients (C_d) of five clusters (A through E; by hierarchical clustering) of 21 sets of fishing gear removed from or similar to those entangling North Atlantic right whales across speeds, at depths of 0 m (solid black), 3 m (dashed black), and 6 m (dotted black). Gray lines illustrate estimated drag coefficients for all gear within that cluster, from which averages are calculated. Note the difference in the *y*-axis limits for panels A, B, C *vs.* D, E.

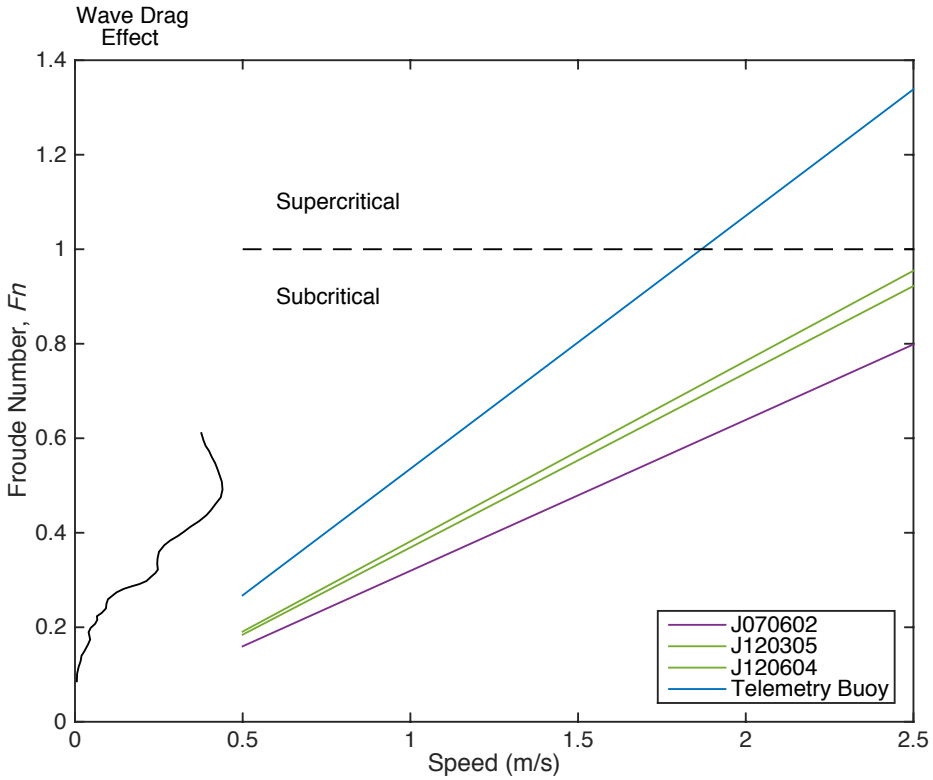

Figure S3. Froude number (*Fn*) with speed (m/s) for three sets of fishing gear removed from entangled right whales (J070602, J120305 and J120604) and the satellite telemetry buoy. Colors represent different gear clusters (see text for details). The magnitude of the wave drag effect is shown for a range of *Fn* (relative; see Lighthill 1978).

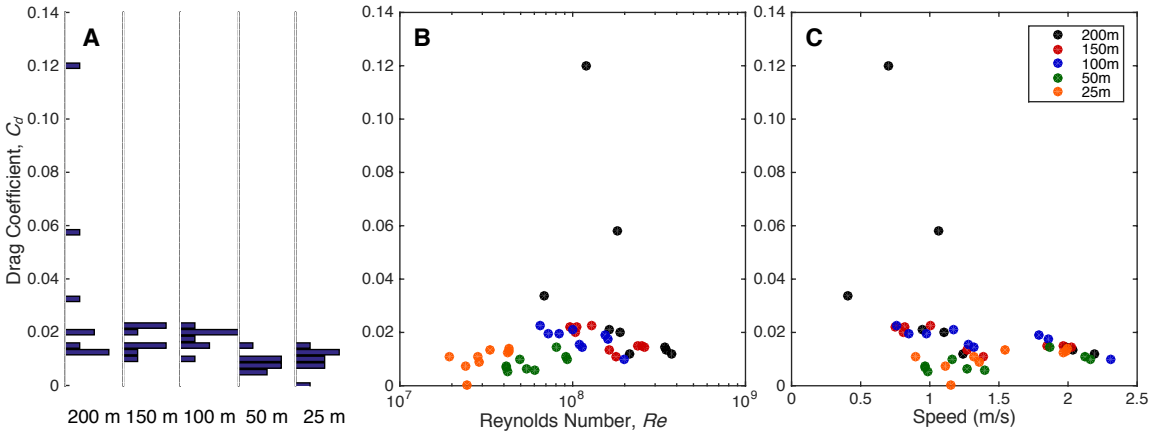

Figure S4. Changes in drag coefficient with towed line length (A), Reynolds number (*Re*; B), and speed (C).

Appendix S2. Estimating wetted surface area and Froude number of gear configurations.

Wetted Surface Area Estimates

Wetted surface area was estimated based on the area of a cylinder with a specified length, l, and radius, *r*:

$$A_w = 2\pi rl \quad \text{(A.1)}$$

For most gear sets, this calculation was straightforward and based on the single line diameter and dimensions; however, for the following six gear sets made up of multiple line types, floats, or buoys, total wetted surface area was estimated as the sum of surface areas of the components of each gear set. For all attached floats and buoys, half the wetted surface area is calculated, assuming that half of each item is in contact with the water.

J070602

Gear details:

Imperial: 121 ft of 3/8" diameter line, with two 32" × 7/8" buoy sticks and an 8" trawl can buoy

Metric: 37 m of 9.5 mm diameter line, with two 813 mm × 22 mm buoy sticks and a 203 mm trawl can buoy

Line $A_w = 2\pi(0.0048\text{ m})(37\text{ m}) = 1.12\text{ m}^2$

Buoy $A_w = \left(\frac{\pi(0.203\text{ m})^2}{2}\right) = 0.0647\text{ m}^2$

Buoy Sticks $A_w = 2\left(\frac{2\pi(0.0111\text{ m})(0.813\text{ m})}{2}\right) = 0.113\text{ m}^2$

Total $A_w = 1.30\text{ m}^2$

J120305

Gear details:

Imperial: 41 ft of 5/16" diameter line, 360 ft of 3/8" diameter line, 3 × 10" diameter trawl can buoys

Metric: 12 m of 8 mm diameter line, 110 m of 9.5 mm diameter line, 3 × 250 mm diameter trawl can buoys

Line $A_w = 2\pi(0.0040\text{ m})(12\text{ m}) + 2\pi(0.0048\text{ m})(110\text{ m}) = 3.62\text{ m}^2$

Buoys $A_w = \left(\frac{\pi(0.254\text{ m})^2}{2}\right) \times 3 = 0.30\text{ m}^2$

Total $A_w = 3.92\text{ m}^2$

J120604

Gear details:

Imperial: 24 ft of sinking 3/8" diameter line, 468 ft floating 3/8" line, 18" diameter balloon, 7" × 14" bullet float

Metric: 7 m of sinking 9.5 mm diameter line, 143 m of 9.5 mm diameter line, 45 cm diameter balloon, 17.8 × 35.6 cm bullet float

Line $A_w = 2\pi(0.0048\text{ m})(7\text{ m}) + 2\pi(0.0048\text{ m})(143\text{ m}) = 4.52\text{ m}^2$

Buoy $A_w = \frac{\pi(0.457\text{ m})^2}{2} = 0.328\text{ m}^2$

Float $A_w = \frac{\pi(0.0889\text{ m})^2 + 2\pi(0.0889\text{ m})(0.356\text{ m} - 0.0889\text{ m}) + 2\pi(0.0889\text{ m})^2}{2} = 0.112\text{ m}^2$

Total $A_w = 4.96\text{ m}^2$

J120808

Gear details:

Imperial: 129 ft of 3/8" diameter line, 600 ft of 5/16" diameter line

Metric: 43 m of 9.5 mm diameter line, 200 m of 8 mm diameter line

Line $A_w = 2\pi(0.0048\text{ m})(43\text{ m}) + 2\pi(0.0040\text{ m})(200\text{ m}) = 6.32\text{ m}^2$

Total $A_w = 6.32\text{ m}^2$

J091298

Gear details:

Imperial: 3 × 2 × 1 ft lobster trap, 48 ft of 5/16" line, 30 ft of 11/32" line, with a 6 × 8" acorn float on a 30" Plante spindle.

Metric: 0.91 × 0.61 × 0.30 m lobster trap, 15 m of 8 mm diameter line, 9 m of 9 mm diameter line, with a 15 × 20 cm acorn float on a 76 cm Plante spindle.

Line $A_w = 2\pi(0.004\text{ m})(15\text{ m}) + 2\pi(0.0044\text{ m})(9\text{ m}) = 0.63\text{ m}^2$

Buoy A_w, assuming the buoy is a half ellipsoid with a = 0.101 m; b = c = 0.076 m using Knud Thomsen's formula, where $p = 1.6075$, =

$$SA \cong \frac{4\pi\left(\frac{a^p b^p + a^p c^p + b^p c^p}{3}\right)^{\frac{1}{p}}}{2} = 0.0446\text{ m}^2$$

Spindle $A_w = 2\pi(0.0127\text{ m})(0.5588\text{ m}) = 0.0448\text{ m}^2$

Total float $A_w = \frac{0.448 + 0.446}{2} = 0.0447\text{ m}^2$

Trap A_w, assuming 0.038 m (1.5") mesh size and 0.0025 m (1/10") wire diameter:
The trap consists of six panels, two each of (a) 0.91 × 0.61 m, (b) 0.61 x 0.30 m, and (c) 0.91 x 0.30 m. The mesh area (A_M) of each panel (a, b, c) was calculated as:

$A_M = N \times K \times 2M \times W$,

where N is number of wire columns, K is number of wire rows, M is the mesh size and W the wire diameter. The number of columns and rows is determined by the size of the panel divided by the mesh size (Fridman and Dvernik 1973, Reid 1977).

$Aw \cong 2\big((24 \times 16) + (16 \times 8) + (24 \times 8)\big) \times 2 \times 0.038\ \text{m} \times 0.0025\ \text{m} = 0.268\ \text{m}^2$

Total $A_w = 0.6258 + 0.0447 + 0.268 = 0.9385\ \text{m}^2$

J051099
Gear details:
Imperial: 216 ft of 1/2" diameter line and 5 ft of 5/8" diameter line, with a gillnet towed in an approximately 3 × 1.5 × 1.5 ft shape.
Metric: 66 m of 12.7 mm, and 2 m of 16 mm diameter line, with a gillnet towed in an approximately 1 × 0.5 × 0.5 m shape.

Line $A_w = 2\pi(0.00635\ \text{m})(66\ \text{m}) + 2\pi(0.0079\ \text{m})(2\ \text{m}) = 2.73\ \text{m}^2$

Gillnet $A_w = 2.5\ \text{m}^2$

Total $A_w = 2.73 + 2.5 = 5.23\ \text{m}^2$

Telemetry Buoy
Gear details:
Imperial: 14" diameter buoy towed on 62 ft of 5/16" diameter line
Metric: 35.6 cm diameter buoy towed on 19 m of 8 mm diameter line

Line $A_w = 2\pi(0.0040\ \text{m})(19\ \text{m}) = 0.478\ \text{m}^2$

Buoy $A_w = \frac{\pi(0.356\ \text{m})^2}{2} = 0.199\ \text{m}^2$

Total $A_w = 0.677\ \text{m}^2$

Froude Number Estimates

The Froude number (*Fn*; dimensionless) was calculated for floats on certain gear sets across the range of measured tow speeds (*U*; m/s) as

$$Fn = \frac{U}{\sqrt{gl}},$$

where *g* is the acceleration due to gravity (9.8 m/s^2) and *l* is the length of the float (m) at the water line level, assuming that each float is half submerged.

J070602: two 0.8 m buoy sticks and an 0.2 m diameter trawl can, total $l = 1.0$ m.

J120305: 3 x 0.25 m diameter trawl can buoys, total $l = 0.75$ m.

J120604: 0.178 m × 0.356 m bullet float that we assume floats at an angle and therefore has $l = 0.25$ m and a 0.45 m diameter balloon float, total $l = 0.7$ m.

Telemetry Buoy: 0.356 m diameter buoy, l = 0.356 m.

Appendix S2. Sets of fishing gear removed from entangled North Atlantic right whales used in this experiment.


J070602


JOS1099


J091298


J092706


J011409


JC13109


J072199


J072498


J071202


J020709

J120604


J120305


J120808


J081800